

**Mechanistic study of methanol synthesis from CO₂ and H₂ on a modified
model Mo₆S₈ cluster**

Cheng Liu¹ and Ping Liu^{2,*}

¹ Mechanical Engineering college, Yangzhou University, 196 Huayang West road, Yangzhou,

Jiangsu 225127, P. R. China

² Chemistry Department, Brookhaven National Laboratory, Upton, New York 11973, USA

Keywords: CO₂ activation, Methanol, Modified molybdenum sulfide, Alkali metal, DFT

* Corresponding author: P. Liu, E-mail: pingliu3@bnl.gov

Abstract

We report the methanol synthesis from CO_2 and H_2 on metal ($\text{M} = \text{K}, \text{Ti}, \text{Co}, \text{Rh}, \text{Ni},$ and Cu)-modified model Mo_6S_8 catalyst using density functional theory (DFT). The results show that the catalytic behavior of a Mo_6S_8 cluster is changed significantly due to the modifiers, via the electron transfer from M to Mo_6S_8 and therefore the reduction of the Mo cation (ligand effect) and the direct participation of M in the reaction (ensemble effect) to promote some elementary steps. With the most positively charged modifier, the ligand effect in the case of $\text{K-Mo}_6\text{S}_8$ is the most obvious among the systems studied; however it cannot compete with the ensemble effect, which plays a dominant role in determining activity via the electrostatic attraction in particular to stabilize the CH_xO_y species adsorbed at the Mo sites of Mo_6S_8 . In comparison, the ligand effect is weaker and the ensemble effect is more important when the other modifiers are used. In addition, the modifiers also vary the optimal reaction pathway for methanol synthesis on Mo_6S_8 , ranging from the reverse water-gas shift (RWGS) + CO hydrogenation as that of Mo_6S_8 to the formate pathway. Finally, K is able to accelerate the methanol synthesis on Mo_6S_8 the most; while the promotion by Rh is relatively small. Using the modifiers like $\text{Ti}, \text{Co}, \text{Ni},$ and Cu , the activity of Mo_6S_8 is decreased instead. The relative stability between $^*\text{HCOO}$ and $^*\text{HOCO}$ is identified as a descriptor to capture the variation in mechanism and scales well with the estimated activity. Our study not only provides better understanding of the reaction mechanism and activities on the modified Mo_6S_8 , but also predicts some possible candidates, which can be used as a promoter to facilitate the CH_3OH synthesis on Mo sulfides.

1. Introduction

Carbon dioxide (CO₂) recycling as a feedstock for producing chemicals contributes to hinder the greenhouse effect caused by the increasing CO₂ emissions. Hydrogenation of CO₂ to synthesize methanol (CO₂ + 3H₂ → CH₃OH + H₂O) has attracted considerable interests.¹⁻⁵ This reaction is of great industrial importance because CH₃OH has been proposed as an alternative energy source^{6,7} and is an important resource to synthesize organic compounds.⁸ The overall conversion in gas-phase is an exothermic reaction ($\Delta H^0 = -49$ kJ/mol), and is merely inhibited by kinetics. Hence, the performance of the catalyst is of great importance to accelerate the kinetics of the process.

Cu-ZnO/Al₂O₃ catalyst is used in industry to produce CH₃OH from syngas mixture (CO-CO₂-H₂) over at 493-573 K and 5-10 MPa;^{9,10} However, the conversion is kinetically limited to 15%-25%.² Extensive efforts have been devoted to investigate the underlying reaction mechanism on Cu and Cu-based systems.^{4,11-15} In contrast, little attention has been paid to Mo compound-based catalysts.¹⁶⁻¹⁸ Bare MoS₂ nanoparticles and edge surfaces convert syngas only to hydrocarbons.^{19,20} The promoters are found necessary for the higher sulfur- and coke-resistance, and better selectivity to higher alcohols.²¹ Differently, our previous study showed that by adopting a unique conformation a model Mo₆S₈ cluster displayed high selectivity to CH₃OH and the CH₃OH production was likely to be higher than pure Cu, while the cluster both in gas phase and supported on Au(111) stayed intact in interaction with the adsorbates.²² However, the overall conversion of CO₂ was much lower than that of MoS₂, which was associated with weaker binding and therefore higher barrier for bond breaking due to the higher S/Mo ratio.

In the present paper, DFT calculations were performed to investigate the CH₃OH synthesis from CO₂ and H₂ on a model Mo₆S₈ cluster modified by various metals (M = K, Ti, Ni, Co, Cu, and Rh), aiming to understand the behaviors of Mo, S and M during the methanol synthesis and improve the activity of Mo₆S₈. On one hand, our study provides better understanding of the reaction mechanism and actives on the modified Mo₆S₈(M-Mo₆S₈); on the other hand, it also predicts some possible candidates, which can be used a promoter to facilitate the CH₃OH synthesis on Mo sulfides.

2. Computational details

Spin-unrestricted DFT calculations for CO₂ hydrogenation to CH₃OH on a M-Mo₆S₈ cluster were conducted using DMol³,^{23,24} which utilized the effective core potentials, double-numerical basis set with polarization functions and GGA-PBE²⁵ for the exchange and correlation functional. A global orbital cutoff of 5.5 Å was used. The modification by adsorbing an adatom of M (M = K, Ti, Ni, Co, Cu, and Rh) was considered, ranging from the alkaline metals to the late transition metals. M-Mo₆S₈ clusters were allowed to fully relax with the adsorbates and no constraints were applied. The binding energy of M on the cluster was expressed as $E(\text{M-Mo}_6\text{S}_8) - E(\text{Mo}_6\text{S}_8) - E(\text{M})$, where E represents the total energy of a M-Mo₆S₈ cluster, a Mo₆S₈ cluster and a M adatom in gas-phase, respectively. We tested that the effect of zero point energy corrections, which is less than 0.15 eV for the reaction barriers. Therefore was not included in the present study. The vdW forces were also not considered here for H₂ and CO₂ adsorptions. Our previous calculations using the same method showed that a H₂ molecule well interacted with Mo₆S₈, being able to dissociate spontaneously at the S sites.²² Given that, the pre-adsorbed atomic H rather than H₂ was used currently for all systems studied.

The CO₂ adsorption is quite strong in some of the modified systems like Ti-Mo₆S₈, which leads to a bent O-C-O bond. The CO₂ adsorption is rather weak on Mo₆S₈, K-Mo₆S₈ and Cu-Mo₆S₈; however for none of the systems, the activity-controlling step or the step with the highest activation barrier along the reaction pathway in this case is associated with the CO₂ binding. That is, the possible increasing in CO₂ adsorption energy due to the use of vdW forces is not likely to affect the trend in activity, which is our interest in this study. The transition state (TS) was located by synchronous transit methods²⁶. The Linear Synchronous Transit (LST) was conducted to bracket the maximum between the reactants and products, followed by repeated conjugate gradient minimizations and the Quadratic Synchronous Transit (QST) maximizations until a transition state was located. The convergence thresholds were set as that the root mean square (rms) forces on the atoms were smaller than 0.002 Ha/Å, making sure that tightening the force threshold did not change the energies and the structures. Such method led to the results close to those obtained by eigenvector following methods. Finally, the located TS was confirmed by vibrational frequency calculations. Considering the accuracy of DFT calculations, our interest here is the difference from one system to the next, which is more precise than the absolute values.

3. Result and discussion

3.1 Structure of M-Mo₆S₈

A Mo₆S₈ cluster is highly symmetric in Chevrel phases with a Mo₆ octahedral core and the sulfur atoms located in the faces of the octahedron (Figure 1). Such structure is initially identified in A_xMo₆S₈ or ABMo₆S₈ solid-state compounds^{27,28} and is further confirmed by the recent DFT calculations and experimental studies on mass-selected clusters.^{29,30-32} The selection

of K and Cu as modifying metals is based on the previous studies, where the promoting effects on the activity of MoS_x catalysts are observed.^{21,33} Both Cu and Ni have been found active for converting CO_2 .³⁴ Rh is chosen according to its unique activity for bond breaking and formation in alcohol chemistry.^{21,35-37} Finally, Ti and Co are included to cover the range going from K to Cu in periodic table, which allows us to understand the electronic effect of M to the activity. Different adsorption sites were considered for a M adatom (Figure S1). Our results show all M atoms prefer to adsorb on the surface of a cluster, rather than in the cavity of Mo_6 cage (Figure 1). K prefers the S-S 2-fold site (Figure 1a) together with one electron transfer from K to Mo_6S_8 (K charge: 0.93 e, Figure 2), which leads to the electron accumulations around both Mo and S sites (Figure 3) and the formation of K cation (K^+). The other M atoms favor the hybrid Mo-S-S-Mo 4-fold site (Figure 1b). In all cases, the Mo_6 octahedral core and the bridging S of Mo_6S_8 cluster stay after interacting with M, though the structural distortion at different degrees is observed depending on the M species. Due to the increasing electronegativity going from K to Cu, the decreasing of the charge of M is observed: $\text{K} > \text{Ti} > \text{Co} > \text{Ni}, \text{Cu} > \text{Rh}$, (Figure 2), while in general the corresponding binding energy becomes weaker. One exception is K. Although there is one electron transfer from K to Mo_6S_8 , the interaction between K and Mo_6S_8 is almost as weak as that of Cu with charge of 0.27 e. This is likely due to the electrostatic repulsion between K cation and Mo cation. As a result, among all M studied, K is the only one, which interacts with Mo_6S_8 selectively via S, rather than via both S and Mo (Figure 1). In addition, with the charge transfer decreasing from K to Rh, there are more and more covalent features in the binding between M and Mo_6S_8 . In this case, the charge itself may not be capable to capture the difference in binding energy, rather the orbital overlapping also contributes, which can explain the small scattering for the late transition metals, Ni and Cu.

3.2 Mechanism of methanol synthesis from CO₂ and H₂ on M-Mo₆S₈

Extensive studies have been performed to identify the reaction mechanism of CH₃OH synthesis, in particular on Cu-based catalysts. Five possible reaction pathways have been proposed.⁵ Path 1 is the conventional formate pathway, where the reaction proceeds through the formation of formate (HCOO), dioxomethylene (H₂COO), formaldehyde (H₂CO), methoxy (H₃CO) and the final product, CH₃OH.^{11,38} Path 2 is the modified formate pathway, where the produced HCOO formation is hydrogenated into formic acid (HCOOH) and eventually to produce H₂CO, H₃CO and CH₃OH.³⁹ Path 3 is initiated by the CO₂ dissociation, which is then hydrogenated to produce CH₃OH via HCO, H₂CO and H₃CO intermediates. Path 4 is very similar to Path 3. The only difference is that CO along Path 4 is produced through the reverse water-gas-shift reaction (RWGS, CO₂ + H₂ → CO + H₂O) via the carboxyl (HOCO) intermediate.^{2,11} Path 5 is a H₂O-mediated mechanism, where the HOCO intermediate is also involved.¹⁴ In Path 5, H₂O is the H atom source for hydrogenation and the HOCO intermediate is further hydrogenated to dihydrocarbene (COHOH), which leads to the formation of COH and CH₃OH.

Our previous study showed that CH₃OH synthesis on Mo₆S₈ followed Path 4.²² Both the Mo and S sites participate in the reaction with CO₂, CO and H_xCO_y preferentially binding to the Mo sites, while S-atoms facilitate H-H bond cleavage via by forming relatively strong S-H bonds. Therefore, there is no competition between H₂ and CO₂ adsorptions. The steric hindrance was only observed for H₂ adsorption on Mo₆S₈,²² where the H₂ has to approach Mo₆S₈ straightly toward the Mo sites to make a spontaneous dissociation occur. Since the reaction occurs at relatively high pressure of H₂, it is reasonable to assume that the formation of atomic H from H₂

dissociation should not hinder the overall conversion. Following this idea, we determined the optimal reaction pathway on M-Mo₆S₈ by considering the pre-adsorbed H at the S sites. The results show that M-Mo₆S₈ does not necessarily follow the same reaction path as Mo₆S₈. In general, the adsorbed M can affect the catalytic activity in two ways. One is via electronic or ligand effect, where M modifies the electronic structure of Mo₆S₈, but not directly involved in the reaction; the other is geometric or ensemble effect, where M can act as an active site to catalyze adsorption, dissociation or bond formation.

3.2.1 K-Mo₆S₈

Among all M-Mo₆S₈ studied, KMo₆S₈ is the only system, which follows Path 4 as the case of Mo₆S₈ (Figure 4). As shown in Figure 5, similar to the case of Mo₆S₈ CO₂ favors the Mo site on the K-Mo₆S₈. K⁺ also participates in the binding via an electrostatic interaction, which strengthens the binding by 0.01 eV in comparison with the adsorption at the Mo site away from K (Figure S2a); while the interaction of CO₂ with K alone (Figure S2b) is less stable. Therefore, both ligand and ensemble effects contribute; however, both effects are relatively weak in this case. The corresponding binding is as weak as that at the Mo site of Mo₆S₈ (binding energy, -0.29 eV, Figure 4). There is almost no charge transfer to CO₂ on adsorption. The C-O bond length and the linear O-C-O bond in gas phase stay intact. Due to the weak adsorption of CO₂, the dissociation to *CO and *O is highly activated (reaction energy, 2.34 eV; barrier, 2.07 eV); in contrast, the hydrogenation of *CO₂ to *HOCO is more favorable (reaction energy, 0.31 eV; barrier, 0.50 eV), with a lower barrier than the hydrogenation to HCOO* (barrier, 1.29 eV). Different from the case of CO₂ adsorption, the ensemble effect associated with adding M plays a significant role in selective formation of *HOCO. For *HCOO, only ligand effect contributes (Figure S3) and the corresponding binding is varied by only 0.05 eV compared to that of Mo₆S₈.

Again, a weak ligand effect as the case of CO₂ adsorption is indicated. Differently, for *HOCO, the ligand effect and more importantly the strong ensemble effect contribute (Figure 5), which leads to a stronger binding by -0.52 eV than that of Mo₆S₈. As a result, on K-Mo₆S₈ *HOCO is more stable than *HCOO by 0.16 eV, while *HOCO is less stable than *HCOO by 0.31 eV in the case of Mo₆S₈. Accordingly, the ensemble effect by K is able to stabilize *HOCO intermediate and therefore lower the formation barrier compared to the case of Mo₆S₈ (barrier, 0.82 eV, Figure 4).²²

The H-assisted HOCO* dissociation to *CO and *H₂O displays much lower barrier (0.44 eV) than that of the direct dissociation to *CO and *OH (2.00 eV). Without adding K, 0.69 eV has to be overcome to form *CO on Mo₆S₈. At this stage, the RWGS reaction is completed, which produces *CO for further hydrogenation to produce CH₃OH. Similar to Mo₆S₈, the *CO hydrogenation undergoes *HCO, *H₂CO, *H₃CO and finally *CH₃OH (Figure 5), which releases the energy of 1.26 eV and corresponds to a barrier of 0.74 eV, 0.69 eV, 0.61 eV and 0.34 eV respectively (Figure 4). In addition, the C-O bond scission of H_xCO, which can lead to the production of methane (CH₄), is also hindered on K-Mo₆S₈ as demonstrated for the case of Mo₆S₈.²²

Compared to Mo₆S₈, the modification by K does not affect the reaction intermediates and the reaction pathway involved in the CH₃OH synthesis; however significant changes in energetics are observed. One can see in Figure 4, K is able to stabilize the reaction intermediates and lower the corresponding transition states involving H_xCO_y radicals, whose binding strength strongly depends on the charge transfer from the surface as well as the electrostatic interaction. In comparison, there is much less effect induced by adding M for relatively stable CO₂, CO, H₂O and CH₃OH molecules. The lowered barriers, in particular for the most activated *CO

hydrogenation to $^*\text{HCO}$ as well as the $^*\text{CO}_2$ hydrogenation to $^*\text{HOCO}$ indicates that the activity promotion by K is likely. Our calculations show that the origin of promoting is associated with the ligand effect and the ensemble effect introduced by adding K. The low electronegativity of K allows a full electron transfer to Mo_6S_8 on adsorption. It leads to the reduction of Mo sites (Figure 3) and therefore increased binding activity compared to Mo_6S_8 (Figure 4); however such effect on the energetics is small. In addition, it also produces K^+ , which makes the ensemble effect more effective than the ligand effect. Our results show that K^+ helps to stabilize $^*\text{H}_x\text{CO}_y$ intermediates adsorbed at the Mo sites via the electrostatic interaction between K and the O of $^*\text{H}_x\text{CO}_y$ (Figure 5). In particular, it leads to the high selectivity to $^*\text{HOCO}$ (Figure 5), which promotes the reaction via $^*\text{HOCO}$ and hinders that via $^*\text{HCOO}$. As will be seen below, such effect is also the key to promote the CH_3OH synthesis on Mo_6S_8 .

3.2.2 Ti- Mo_6S_8

In comparison with K- Mo_6S_8 , the ensemble effect plays a more dominant role for CH_3OH synthesis on Ti- Mo_6S_8 . Due to the direct participation of Ti in the reaction, the optimal path varies from Path 4 to Path 3, where the C-O bond cleavage is favored. CO_2 adsorbs at the Mo-Ti bridge site of TiMo_6S_8 (binding energy, -1.32 eV) more strongly than that on K- Mo_6S_8 (Figure 4). Both C and O atoms of CO_2 tightly bind with Ti and Mo, where the C-O bond is elongated by $\sim 0.1 \text{ \AA}$ and the O-C-O is bent by 42.3° , together with 0.36 electron gain from Ti- Mo_6S_8 (Figure 6a). As a consequence of strong CO_2 -Ti interaction, the C-O bond breaking is facilitated on Ti- Mo_6S_8 . The dissociation of $^*\text{CO}_2$ to form $^*\text{CO}$ and $^*\text{O}$ is exothermic (reaction energy, -0.70 eV) and the corresponding barrier is 0.57 eV. The hydrogenation of $^*\text{CO}_2$ to $^*\text{HOCO}$ (barrier, 1.14 eV) and $^*\text{HCOO}$ (barrier, 0.89 eV) can be compatible with the dissociation; in contrast, the H-assisted $^*\text{CO}_2$ dissociation to produce $^*\text{CO}$ and $^*\text{OH}$ is the most preferential with no barrier

(Figure 4). The further hydrogenation of *CO to CH₃OH follows the same pathway as that of K-Mo₆S₈ via *HCO, *H₂CO and *H₃CO. Although thermodynamically these processes (total energy release, 1.16 eV) are comparable with those of KMo₆S₈ in energy; however, kinetically they are less favorable and the corresponding barrier for each elementary step involved is higher, 0.69 eV, 0.95 eV, 0.88 eV, and 1.82 eV, respectively. Especially, the hydrogenation of *H₃CO to *CH₃OH is highly activated (barrier, 1.82 eV) and is likely to slow down the overall CH₃OH production. Again, this is associated with the ensemble effect introduced by adding Ti, which stabilizes the H_xCO intermediates and the transition states (Figure 4) by direct bond formation of Ti with the adsorbate via C and/or O (Figure 6). In addition, we also considered the possibility of C-O bond breaking. Our results show that breaking the C-O of *CO (barrier, 2.67 eV), *HCO (barrier, 2.46 eV), *H₂CO (barrier, 2.32eV), *H₃CO (barrier, 2.29 eV) and *H₃COH (barrier, 2.52 eV) is more difficult than the corresponding hydrogenation. In contrast to the ensemble effect, the ligand effect due to the electron transfer (0.54 e) from Ti to Mo₆S₈ is trivial. For instance, the CO₂ adsorption on top of Mo away from Ti is as weak as that on KMo₆S₈ and Mo₆S₈, which cannot compete with the adsorption on the Ti-Mo bridge site. In fact, when CO₂ is initially positioned on top of Mo next to Ti, the molecule spontaneously shifts to the most stable Ti-Mo bridge site during the geometry optimization.

Upon going from Mo₆S₈ to Ti-Mo₆S₈, the optimal reaction pathway for CH₃OH synthesis varies from Path 4 to Path 3. This is due to the high activity of the adsorbed Ti, which is capable to facilitate CO₂ dissociation and stabilize the various intermediates and transition states. The ensemble effect due to adding Ti plays an essential role, where Ti is involved directly in the binding of an adsorbate, especially for *H₃CO. As a result, a high barrier of 1.82 eV (Figure 4) has to be overcome to produce *CH₃OH via *H₃CO hydrogenation. Compared to both Mo₆S₈

and K-Mo₆S₈, the CH₃OH synthesis on Ti-Mo₆S₈ is rather difficult. Therefore, the catalyst may get poisoned and the activity is decreased (Figure 11). Yet, Ti is not active enough to allow C-O bond breaking of H_xCO and therefore the formation of CH₄ can be hindered.

3.2.3 Co-Mo₆S₈ and Rh-Mo₆S₈

Adding Co and Rh also results in a variation in reaction pathway for CH₃OH synthesis on Mo₆S₈, going from Path 4 to Path 2 (Figure 7). Although Co and Rh are not as active as Ti, the direct participation of Co and Rh in the reaction is also observed (ensemble effect) (Figure 8). *CO₂ favors the Rh-Mo bridge site (Figure 8) with the O-C-O bond bent by 37.4° and the C-O bond elongated by 0.07 Å. The corresponding binding energy is -0.59 eV and the molecule is negatively charged (-0.14 e). The effect of Rh on *CO₂ is very similar, and again less significant compared to the case of Ti-Mo₆S₈, where the C-O breaking is not observed and the H-assisted *CO₂ dissociation to *CO and *OH is highly activated (barrier, 2.02 eV). Alternatively the hydrogenation to *HCOO is favored (barrier, 0.67 eV), while *HOCO is less likely to form (barrier, 1.36 eV). The further hydrogenation of *HCOO produces *HCOOH (barrier, 0.83 eV) and *H₂COOH (barrier, 0.57 eV), which is the precursor for C-O bond breaking to form *H₂CO (barrier, 0.42 eV). The conversion of *H₂CO to *CH₃OH via *H₃CO is exothermic (reaction energy, 0.51 eV and 0.41 eV; barrier, 0.16 eV and 0.77 eV, respectively). One can see in Figure 8, Rh is directly involved in binding process and increases the stability of the reaction intermediates compared to those on Mo₆S₈ (Figure 4). In contrast, the ligand effect due to the electron transfer from Rh (0.16 e) to Mo₆S₈ can be barely seen. The binding energy for an adsorbate at the Mo sites away from Rh is the same as that on Mo₆S₈. Similar energy profile is also observed for Co-Mo₆S₈ (Figure 7). The difference is that the reaction intermediates and transition states involved are more stable on Co-Mo₆S₈ than on Rh-Mo₆S₈. Such difference can

be attributed to higher binding activity of 3d metal Co than 4d metal Rh. According to the energetics (Figure 7), it seems that adding Rh (or even Co) is better than adding Ti for promoting the CH₃OH production on Mo₆S₈.

3.2.4 Ni-Mo₆S₈ and Cu-Mo₆S₈

The CH₃OH synthesis on Ni-, Cu-Mo₆S₈ also follows Path 2 as the cases of Co-Mo₆S₈ and Rh-Mo₆S₈, though different precursor is observed for the C-O bond breaking to produce H_xCO intermediate (Figure 9). Again, the strong ensemble effect is observed. Compared to Ti-, Co-, Rh-Mo₆S₈, the effect of Ni on the binding property of Mo₆S₈ is much less. For CO₂ adsorption, the corresponding binding energy is -0.47 eV on Ni-Mo₆S₈, though the favorable binding conformation at the Mo-Ni bridge site is similar with the O-C-O bond bent by 31.7° and the C-O bond elongated by 0.06 Å (Figure 10a). In presence of hydrogen, *CO₂ is likely to be converted to *HCOO (barrier, 0.71 eV) and sequentially *HCOOH (0.70 eV). Different from the cases of Co-Mo₆S₈ and Rh-Mo₆S₈, *HCOOH is the precursor for C-O bond cleavage (Figure 10b), which produces *HCO (barrier, 0.90 eV); in contrast, the hydrogenation to *H₂COOH is less likely (barrier, 2.09 eV). Finally, *HCO is converted to *CH₃OH via *H₂CO and *H₃CO, which releases energy of 1.46 eV with the barriers less than 0.70 eV. When using Cu as a modifier, Mo₆S₈ is even less affected compared to that of Ni. For CO₂ adsorption, for instance, the adsorption energy at the Cu site (-0.27 eV) and Mo (-0.26 eV) sites are very close, which are weaker than the Ni-Mo₆S₈. *CO₂ is slightly charged and the linear O-C-O conformation stays intact as the cases of Mo₆S₈ and K-Mo₆S₈ (Figure 10c). The reaction on Cu-Mo₆S₈ undergoes the same pathway as Ni-Mo₆S₈ (Figure 10d); however, the stability for reaction intermediates and transition states is much lower. The highest barrier along the reaction pathway for CuMo₆S₈ is 1.45 eV, corresponding to hydrogenation of *HCOO to *HCOOH (Figure 9). This is quite high,

which can obstacle the CH₃OH production; while on RhMo₆S₈, the most activated C-O bond cleavage of *HCOOH is less difficult to overcome (barrier, 0.90 eV).

Our results show that the metal modification can affect the catalytic behavior of Mo₆S₈ toward CH₃OH synthesis significantly. Due to the ligand effect, the Mo cation of Mo₆S₈ is reduced in different degrees, which indirectly affects the binding property of Mo₆S₈. The ensemble effect leads to the directly participation of added metals in the reaction. For all M studied, the ensemble effect plays a major role, which leads to the stabilization of reaction intermediates and transition states involved in CH₃OH synthesis on Mo₆S₈. The ligand effect is the most obvious in the case of K-Mo₆S₈, where K is charged the most positively among all M studied; yet the resulted increase in binding energy on the Mo sites is very small. However, the produced K⁺ allows the strong ensemble effect via the electrostatic attraction, which helps in stabilizing the *H_xCO_y adsorbed at the Mo site. In comparison, the ligand effect is weaker and the ensemble effect is more dominate for the other M-Mo₆S₈ cases, where M donates fewer electrons and binds the adsorbates more strongly than K. In term of M-induced variation in energetics, K shows the least changes along the reaction pathway; while Ti displays the most significant effect, which allows the spontaneous C-O cleavage under hydrogen environments. In addition, the effect by adding M is not only limited to vary the binding property of the catalysts, but also the optimal reaction pathway. In our case, depending on the species of M, three reaction paths are identified, where only K-Mo₆S₈ follows the RWGS via *HOCO intermediate + CO hydrogenation as that of Mo₆S₈. The reaction pathway for Ti-Mo₆S₈ is similar, but the RWGS undergoes via direct H-assisted CO₂ dissociation. For the other systems, the formate pathway via *HCOO and *HCOOH is favored.

3.3 Activity of M-Mo₆S₈ toward methanol synthesis

Now the question is how the variation in the energetics affects the overall conversion. The rate of CH₃OH synthesis with respect to Mo₆S₈ is estimated according to $e^{\frac{-(E_a^{max} - E_a^{max, Mo_6S_8})}{k_B T}}$, where E_a^{max} represents the highest reaction barrier along the optimal reaction path identified above (arrows in Figures 4, 7, 9) and T is temperature, 525 K in this case. This is based on the assumption that the step with the highest barrier along the reaction pathway is the most likely to slow down the overall conversion. Our previous calculations showed that the estimation of the overall reaction rate using E_a^{max} was able to capture the difference in activity measured experimentally for CH₃OH synthesis on Cu(111) and Cu/ZnO.¹¹ The success of such estimation has also been reported for the oxygen reduction reaction on metal surfaces.⁴⁰ In addition, for all 7 cases studied same coverage of CO₂ (one CO molecule per cluster) was applied and therefore the calculated E_a^{max} should be comparable. Here, the desorption process was not considered for selecting E_a^{max} . Since the reaction occurs at relatively high temperature 500K-600K, the desorption will be strongly affected considering the effect of entropy. For example, the barrier to desorb H₂O from Mo₆S₈ can be compensated by the energy gain from TΔS at 525 K (Figure 4); in contrast for the TS3 associated with the highest barrier step, both the reactant and the product are adsorbed species and therefore the effect of TΔS is much smaller. As shown in Figure 11, the rate for CH₃OH yield decreases in a sequence: K-Mo₆S₈ > Rh-Mo₆S₈ > Mo₆S₈ > Ni-Mo₆S₈ > Co-Mo₆S₈ > Cu-Mo₆S₈ > Ti-Mo₆S₈. Among the systems studied, K is able to promote CH₃OH production the most, while the promotion by Rh is relatively small. On the contrary, the activity of Mo₆S₈ is slightly decreased when modified by Ni and Co and is significantly degraded when using Cu or Ti. Previously, we performed similar calculations to study CH₃OH synthesis on Cu₂₉ and Cu(111).¹¹ To compare with Mo₆S₈-based systems, E_a^{max} for both Cu₂₉ (1.41 eV) and

Cu(111) (1.60 eV) were used to estimate the CH₃OH production at 525 K. One can see in Figure 11 that bare Mo₆S₈ cluster as well as the cluster modified by K, Rh, Ni and Co can display higher activity in CH₃OH production than Cu in an increasing sequence: Cu(111) < Cu₂₉ < Co-Mo₆S₈ < Ni-Mo₆S₈ < Mo₆S₈ < Rh-Mo₆S₈ < K-Mo₆S₈. E_a^{max} is lowered from 1.60 eV for Cu(111) to 0.74 eV for K-Mo₆S₈ (~10⁸ increase in CH₃OH production rate) and the corresponding step varies from *HCOO hydrogenation via formate mechanism to *CO hydrogenation via RWGS + CO hydrogenation mechanism. In fact, E_a^{max} identified for K-Mo₆S₈ is close to that for Cu/CeO_x/TiO₂ (0.66 eV) from our recent study, which has been reported recently as a highly efficient catalyst for CH₃OH synthesis from CO₂.¹⁵ Accordingly, the corresponding rate for CH₃OH production on K-Mo₆S₈ is only 5 times slower than that on Cu/CeO_x/TiO₂. Therefore, Mo₆S₈ and Mo₆S₈ modified by K, Rh, Co, and Ni are likely to be a good catalyst for converting CO₂ to CH₃OH.

According to sabatier's principle, a good catalyst should provide a moderate binding, strong enough to adsorb and dissociate the reactants and weak enough to allow the formation and removal of products from the catalyst.⁴¹ The promotion by K for the CH₃OH synthesis on Mo₆S₈ is dominated by the ensemble effect, while the ligand effect plays relatively small role. Due to the low electronegativity, K⁰ transforms into K⁺ when adsorbed on Mo₆S₈. More importantly, K⁺ helps to moderate the stability of *H_xCO_y intermediates adsorbed at the Mo sites via electrostatic interaction as well as lower the corresponding activation barriers (Figure 4 and Figure 5). In addition, the S sites also participate in the reaction by stabilizing the dissociated H. Therefore, the overall high activity of K-Mo₆S₈ is attributed to the synergy among K, Mo and S sites. Similar situation is observed for Rh-Mo₆S₈. Like K⁺, the direct participation of Rh (ensemble effect) also helps to stabilize the reaction intermediates and transition states as compared to

Mo₆S₈ (Figure 7). Since Rh has the much lower electronegativity than K and is less positively charged on interaction with Mo₆S₈ (Figure 2), the increased stability in the case of Rh-Mo₆S₈ is not due to the electrostatic interaction, but the direct charge transfer from Rh to the adsorbates. As a result, the stabilization provided by Rh is much stronger than that by K⁺. In fact, the binding is too strong to allow the hydrogenation to occur as efficient as that of K-Mo₆S₈, and therefore the lower activity is predicted (Figure 11). Given that, the amount of M should be appropriate. The over-dose of K or Rh may over-activate the Mo sites via the ligand effect and/or poison the active Mo and S sites.

The observed trend in CH₃OH production rate can be well explained by the difference in binding energy between *HOCO and *HCOO (Figure 11). In general, the five reaction pathways shown above can be grouped into two major reaction mechanisms. Path 1-2 correspond to the formate mechanism via *HCOO intermediate. Path 3-5 correspond to the RWGS + CO hydrogenation mechanism via *HOCO intermediate. Therefore, the relative stability between HCOO and HOCO, $E_{\text{ads}}(\text{HOCO}) - E_{\text{ads}}(\text{HCOO})$, is likely to differentiate the mechanism. Indeed, our results show that for Ti-Mo₆S₈, K-Mo₆S₈ and Mo₆S₈, the value of $E_{\text{ads}}(\text{HOCO}) - E_{\text{ads}}(\text{HCOO})$ is either negative or close to zero and the RWGS + CO hydrogenation mechanism is favored for CH₃OH synthesis (Figure 11). Note that in the case of Ti-Mo₆S₈, *HOCO is not stable and the energy for the dissociated *OH and *CO is used instead. Within the RWGS + CO hydrogenation mechanism, a volcano-like trend is observed. An effective promoter, e.g. K, should be able to decrease the value of $E_{\text{ads}}(\text{HOCO}) - E_{\text{ads}}(\text{HCOO})$ in the case of Mo₆S₈ slightly to achieve higher CH₃OH yield. With the major contribution from the ensemble effect, adding K is able to stabilize *HOCO more significant for than that for *HCOO (Figure 5). The K-promoted stabilization via the ensemble effect is not only for *HOCO, but also for the other H_xCO species, including

*HCO involved in the most highly activated step. As a result, the corresponding barrier is lowered and higher CH₃OH production is predicted (Figure 4 and Figure 11). Over-stabilizing *HOCO on Ti-Mo₆S₈ via the direct participation of Ti (ensemble effect) not only leads to the facile C-O bond cleavage, but also results in the poisoning of the catalyst. The binding that Ti provides is too strong and the formation of CH₃OH from *H₃CO has to overcome a high barrier (Figure 4). Therefore, the catalyst may get poisoned and the activity is decreased (Figure 11). With more positive value of E_{ads}(HOCO) - E_{ads}(HCOO), the formate pathway is adopted. An decreasing in activity, Rh-Mo₆S₈ > Ni-Mo₆S₈ > Co-Mo₆S₈ > Cu-Mo₆S₈, with the increasing value of E_{ads}(HOCO)- E_{ads}(HCOO) is observed (Figure 11). Accordingly, a promoter which is able to minimize the value of E_{ads}(HOCO) - E_{ads}(HCOO) should be considered for improving the activity of Mo₆S₈.

Finally, as shown in Figures 5, 6, 8, 10, Mo₆S₈ and M-Mo₆S₈ clusters display a reasonable stability under the reaction conditions. The interactions with OH, H₂O, and other reaction intermediates only lead the distortion of the clusters, while the Mo₆ octahedral core stays during the reaction. Besides, the previous experiments on mass-selected MoS_x clusters also showed that such sub-nanometer clusters were able survive in reaction with CO and NH₃.^{32,42} Are K and Rh, which promote the activity of Mo₆S₈, also likely to survive under the reaction conditions? As shown in Figure 5, by losing one electron K⁺ does not interact with the reaction intermediates alone but promoting the stability of the H_xCO_y species adsorbed at the Mo sites via the electrostatic interaction. In addition, considering the step with the highest barrier on KMo₆S₈ (Figure 4), the possible CO accumulation may be expected, which does not poison the K sites, but the Mo sites (Figure 5). Therefore, K is likely to survive, which has been observed for MoS₂-based catalysts.²¹ For Rh, the site block or oxidation by *HCOO (Figure 8) should be

considered due to the highly activated $^*\text{HCOO}$ hydrogenation on Rh-Mo₆S₈ (Figure 7). Further detailed study under more realistic reaction conditions should be carried out to gain better understanding of the catalyst stability. To make the M-Mo₆S₈ clusters the more practical catalysts, a support can be considered. Previously, we have shown both experimentally and theoretically that a Mo₆S₈ cluster can be successfully landed on Au(111) surface and the activity of active sites remains the same on deposition.²² Accordingly, the similar activity for M-Mo₆S₈ cluster on supports can be expected.

4. Conclusion

DFT calculations were employed to investigate the effect of a model Mo₆S₈ catalyst modified by K, Ti, Co, Rh, Ni, and Cu (M-Mo₆S₈) toward the CH₃OH synthesis from CO₂ and H₂. The present study shows that metal modification can affect the catalytic behavior of a Mo₆S₈ cluster significantly, via the ligand effect and the ensemble effect. With the most positively charged M, the ligand effect in the case of K-Mo₆S₈ is the most obvious among all systems studied; yet the resulted increase in binding energy on the Mo sites is very small. However, the produced K⁺ allows the strong ensemble effect via the electrostatic attraction, which helps in stabilizing the $^*\text{H}_x\text{CO}_y$ adsorbed at the Mo site. In comparison, the ligand effect is weaker and the ensemble effect seems more dominant for the other M-Mo₆S₈. Compared to Mo₆S₈, adding K shows the least changes in energy along the reaction pathway; while Ti displays the most significant effect, which allows the spontaneous C-O bond cleavage under the hydrogen environments. The addition of M also varies the optimal reaction pathway on Mo₆S₈. In our case, depending on the species of M, three reaction paths are identified. Only K-Mo₆S₈ follows the RWGS via $^*\text{HOCO}$ intermediate + CO hydrogenation as that of Mo₆S₈. Similar pathway is also

adopted on Ti-Mo₆S₈, except that the RWGS undergoes via direct H-assisted CO₂ dissociation. For the other M-Mo₆S₈ systems studied, the formate pathway via *HCOO and *HCOOH is favored.

Our calculations show that Mo₆S₈ cluster as well as the clusters modified by K, Rh, Ni and Co can display higher activity in CH₃OH production than Cu in an increasing sequence: Ti-Mo₆S₈ < Cu-Mo₆S₈ < Cu(111) < Cu₂₉ < Co-Mo₆S₈ < Ni-Mo₆S₈ < Mo₆S₈ < Rh-Mo₆S₈ < K-Mo₆S₈. K is able to accelerate the CH₃OH synthesis from CO₂ and H₂ on Mo₆S₈ the most among the systems studied; while the promotion by adding Rh is relatively small. Using the metal like Ti, Co, Ni and Cu, the activity of Mo₆S₈ is decreased instead. The relative stability between *HCOO and *HOCO, $E_{\text{ads}}(\text{HOCO}) - E_{\text{ads}}(\text{HCOO})$, is identified as a descriptor, being able to differentiate the mechanism and scale well with the estimated activity of the M-Mo₆S₈. Negative or neutral $E_{\text{ads}}(\text{HOCO}) - E_{\text{ads}}(\text{HCOO})$ favors the RWGS + CO hydrogenation mechanism, while the positive value results in the formate mechanism. Within the RWGS + CO hydrogenation mechanism, an effective promoter, e.g. K, should be able to decrease the value of $E_{\text{ads}}(\text{HOCO}) - E_{\text{ads}}(\text{HCOO})$ on Mo₆S₈ slightly to achieve higher CH₃OH production. Over-stabilizing *HOCO, e.g. Ti, leads to the poisoning of the catalyst. Along the formate mechanism, a promoter should minimize the value $E_{\text{ads}}(\text{HOCO}) - E_{\text{ads}}(\text{HCOO})$ for achieving higher activity. The overall high activity of KMo₆S₈ is attributed to the synergy among K, Mo and S sites. Our results not only provides better understanding of the reaction mechanism and actives on the modified Mo₆S₈, but also predicts some possible candidates, which can be used a promoter to facilitate the CH₃OH synthesis on Mo sulfides.

Acknowledgment

Part of the research was carried out at Brookhaven National Laboratory under contract DE-AC02-98CH10886 with the U. S. Department of Energy, Office of Science, Office of Basic Energy Sciences, Division of Chemical Sciences. Part of the DFT calculations was carried out at Centers for Functional Nanomaterials at Brookhaven National Laboratory. C. L. would like to thank the funding from the International industry-university-research project # YZ2012061.

Captions

Figure 1 Optimized structures for M-Mo₆S₈ clusters. (a) M at the S-S 2-fold site; (b) M at the S-Mo-Mo-S 4-fold site. Big purple or grey: M; big cyan: Mo; small yellow: S.

Figure 2 Calculated charge and binding energy of M atom adsorbed on Mo₆S₈.

Figure 3 Calculated total electron density mapped by the electrostatic potential of a Mo₆S₈ cluster before and after modification by M. The isosurface value is 0.05eÅ⁻³. Electrostatic potential is color coded as follows: the blue corresponds to negatively charged regions, while the red represents positively charged regions.

Figure 4 Optimal potential energy diagrams for methanol synthesis on K-, Ti-Mo₆S₈ clusters including reaction intermediates (thin bar) and transition states (TS, thick bar). Mo₆S₈ was also included for comparison, which was cited from Ref.²². The arrow pointed to the step with the highest barrier.

Figure 5 Geometries of the reaction intermediates and transition states (TS) involved in a for methanol synthesis on a K-Mo₆S₈ cluster. Big purple: K; big cyan: Mo; small yellow: S; small red: O; small white: H; small grey: C.

Figure 6 Geometries of some reaction intermediates involved in a for methanol synthesis on a Ti-Mo₆S₈ cluster. (a) *CO₂; (b) *HCO; (c) *H₂CO; (d) *H₃CO. Big grey: Ti; big cyan: Mo; small yellow: S; small red: O; small white: H; small grey: C.

Figure 7 Optimal potential energy diagrams for methanol synthesis on Rh-, Co-Mo₆S₈ clusters including reaction intermediates (thin bar) and transition states (TS, thick bar). The arrow pointed to the step with the highest barrier.

Figure 8 Geometries of the reaction intermediates and transition states (TS) involved in a for methanol synthesis on a Rh-Mo₆S₈ cluster. Big brown: Rh; big cyan: Mo; small yellow: S; small red: O; small white: H; small grey: C.

Figure 9 Optimal potential energy diagrams for methanol synthesis on Ni-, Cu-Mo₆S₈ clusters including reaction intermediates (thin bar) and transition states (TS, thick bar). The arrow pointed to the step with the highest barrier.

Figure 10 Geometries of some reaction intermediates involved in a for methanol synthesis on Ni-Mo₆S₈ and Cu-Mo₆S₈ clusters. (a) *CO₂/Ni-Mo₆S₈ (b) *HCO + *H₂O/Ni-Mo₆S₈; c) *CO₂/Cu-Mo₆S₈ (d) *HCO + *H₂O/Cu-Mo₆S₈. Big blue: Ti; big light brown: Cu; big cyan: Mo; small yellow: S; small red: O; small white: H; small grey: C.

Figure 11 Variation of the relative rate for methanol synthesis with the difference in binding energy between HOCO and HCOO on Mo₆S₈ and various M-Mo₆S₈ clusters, where the rate was

expressed with respect to that of Mo₆S₈. The data point for Cu₂₉ and Cu(111) was also included according to Ref.¹¹ for reference.

Supporting Information. Optimized structures of modified Mo₆S₈ clusters with and without interaction with an adsorbate together with the corresponding energetics This material is available free of charge via the Internet at <http://pubs.acs.org>.

Reference

- (1) Ma, J.; Sun, N.; Zhang, X.; Zhao, N.; Xiao, F.; Wei, W.; Sun, Y. *Catal. Today* **2009**, *148*, 221.
- (2) Liu, X. M.; Lu, G. Q.; Yan, Z. F.; Beltramini, J. *Ind. Eng. Chem. Res.* **2003**, *42*, 6518.
- (3) Song, C. *Catal. Today* **2006**, *115*, 2.
- (4) Behrens, M.; Studt, F.; Kasatkin, I.; Kühl, S.; Hävecker, M.; Abild-Pedersen, F.; Zander, S.; Girgsdies, F.; Kurr, P.; Knief, B.-L.; Tovar, M.; Fischer, R. W.; Nørskov, J. K.; Schlögl, R. *Science* **2012**, *336*, 893.
- (5) Liu, P.; Yang, Y.; White, M. G. *Surf. Sci. Rep.* **2013**, *68*, 233.
- (6) Olah, G. A. *Angew. Chem. Int. Ed.* **2005**, *44*, 2636.
- (7) Olah, G. A.; Goepfert, A.; Prakash, G. K. S. *Beyond Oil and Gas: The Methanol Economy*; 2nd ed.; Wiley-VCH: Weinheim, 2009.
- (8) Xu; Moulijn, J. A. *Energy & Fuels* **1996**, *10*, 305.
- (9) Waugh, K. C. *Catal. Today* **1992**, *15*, 51.
- (10) Chinchen, G. C.; Denny, P. J.; Parker, D. G.; Spencer, M. S.; Whan, D. A. *Appl. Catal.* **1987**, *30*, 333.
- (11) Yang, Y.; Evans, J.; Rodriguez, J. A.; White, M. G.; Liu, P. *Phys. Chem. Chem. Phys.* **2010**, *12*, 9909.
- (12) Yang, Y.; White, M. G.; Liu, P. *J. Phys. Chem. C* **2012**, *116*, 248.
- (13) Yang, Y.; Mims, C. A.; Mei, D. H.; Peden, C. H. F.; Campbell, C. T. *J. Catal.* **2013**, *298*, 10.
- (14) Zhao, Y.-F.; Yang, Y.; Mims, C.; Peden, C. H. F.; Li, J.; Mei, D. *J. Catal.* **2011**, *281*, 199.
- (15) Graciani, J.; Mudiyansele, K.; Xu, F.; Baber, A. E.; Evans, J.; Senanayake, S. D.; Stacchiola, D. J.; Liu, P.; Hrbek, J.; Sanz, J. F.; Rodriguez, J. A. *Science* **2014**, *345*, 546.
- (16) Herman, R. G. *Catal. Today* **2000**, *55*, 233.
- (17) Wang, W.; Wang, S.; Ma, X.; Gong, J. *Chem. Soc. Rev.* **2011**, *40*, 3703.

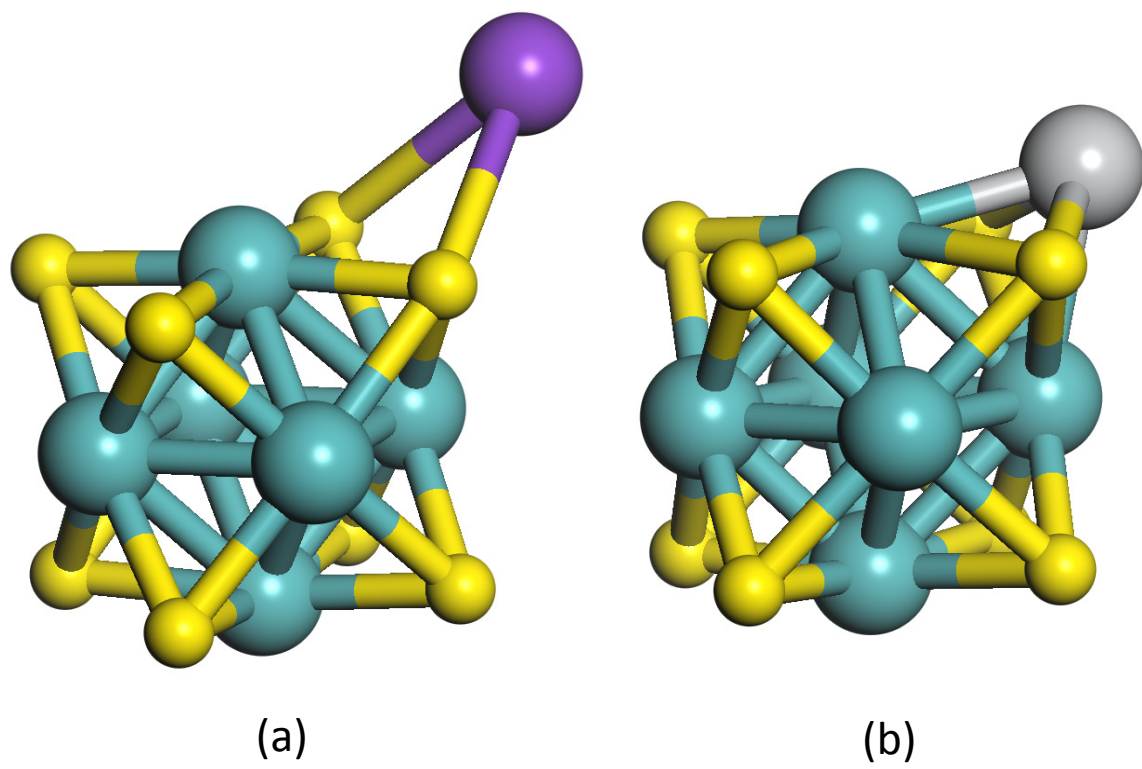


Figure 1

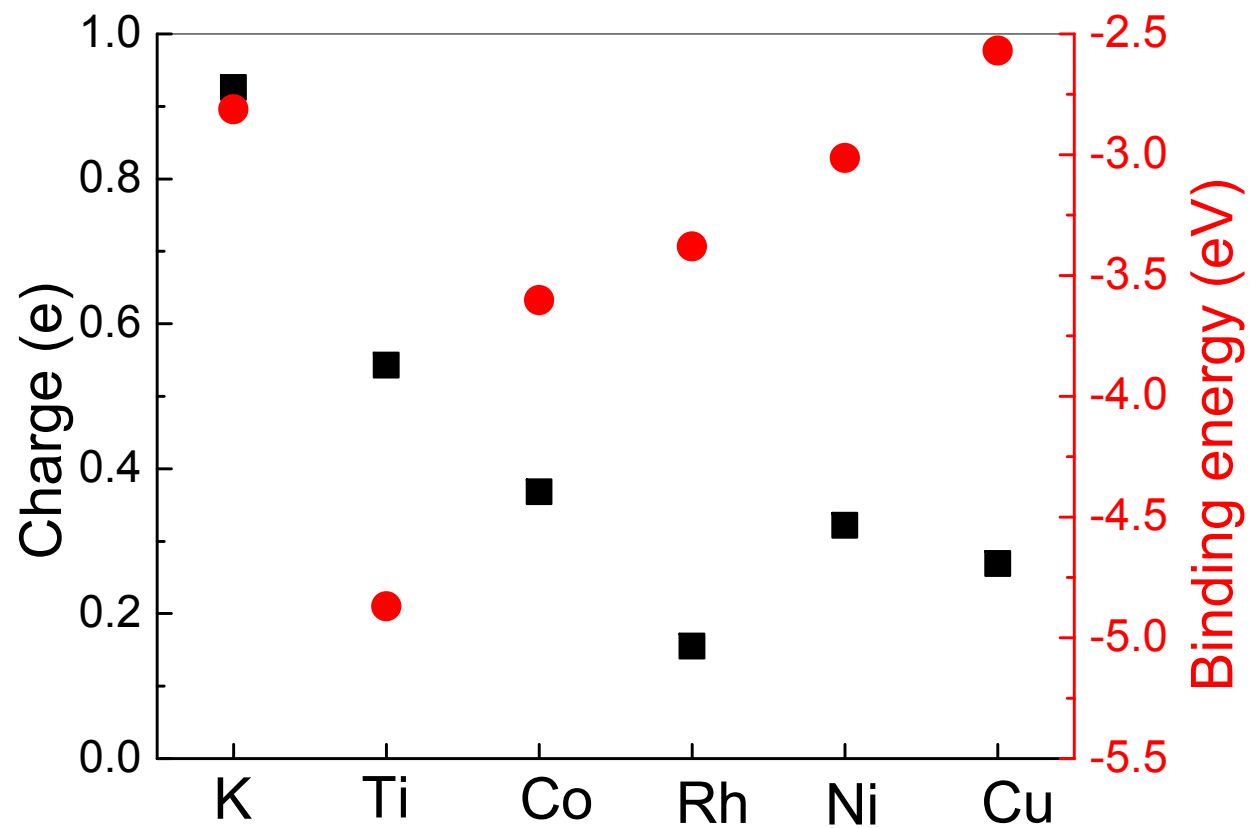


Figure 2

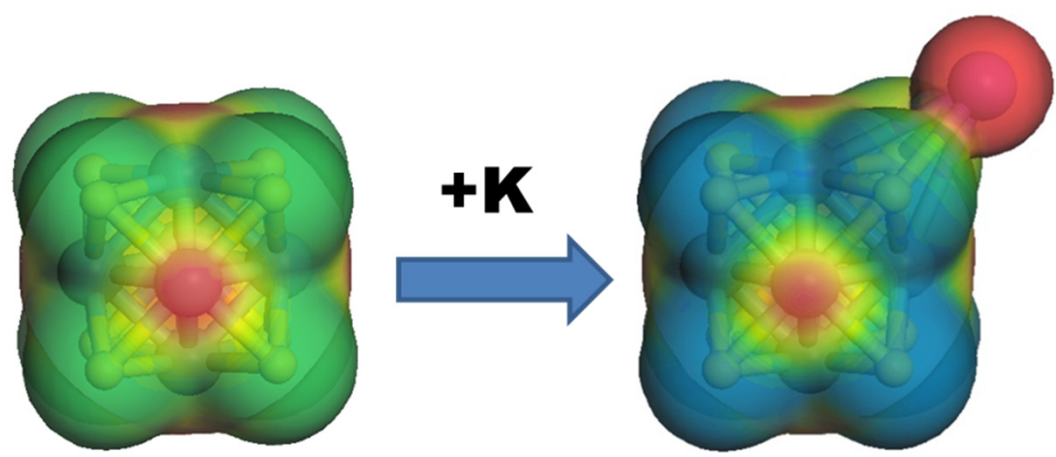


Figure 3

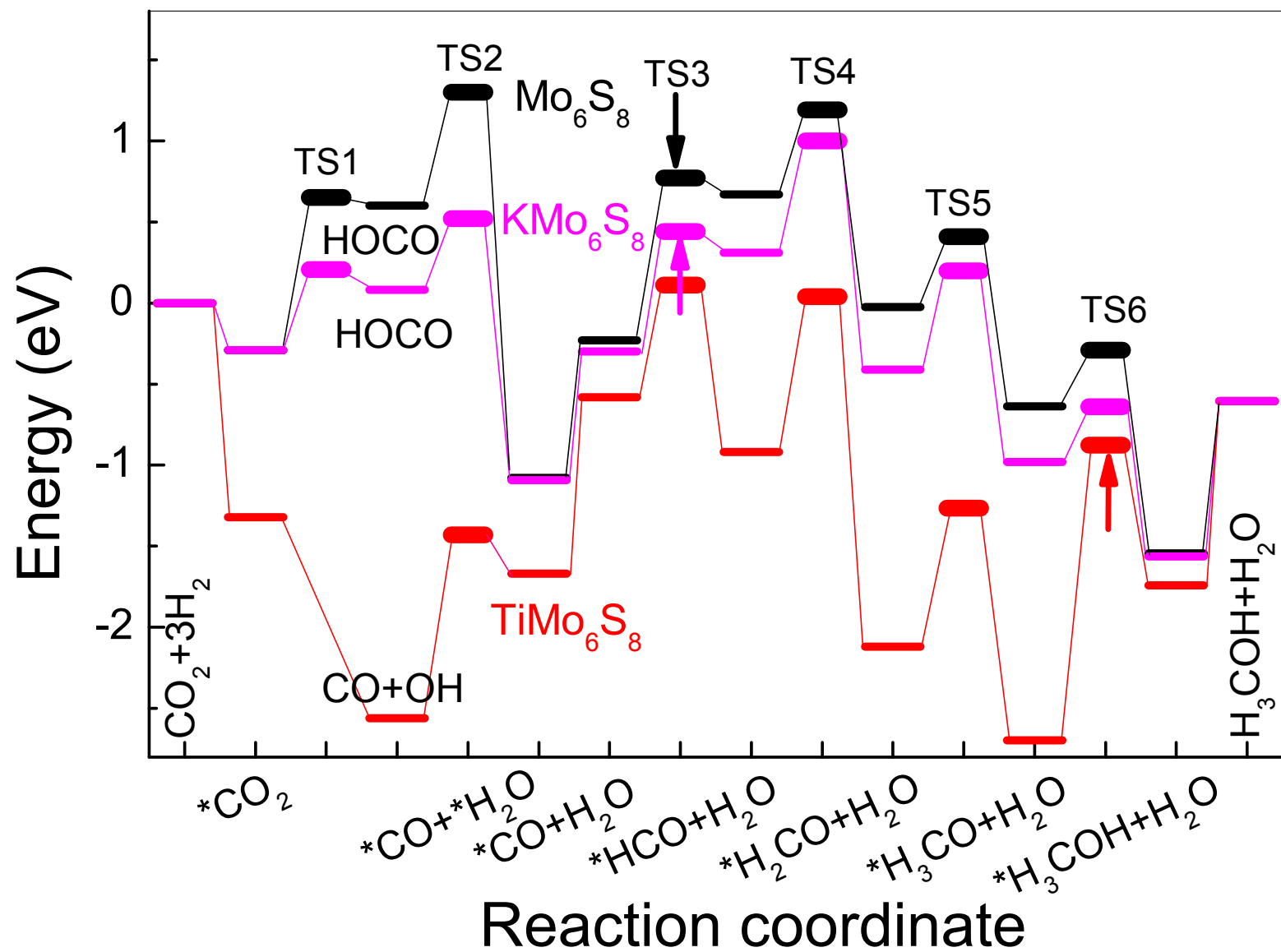


Figure 4

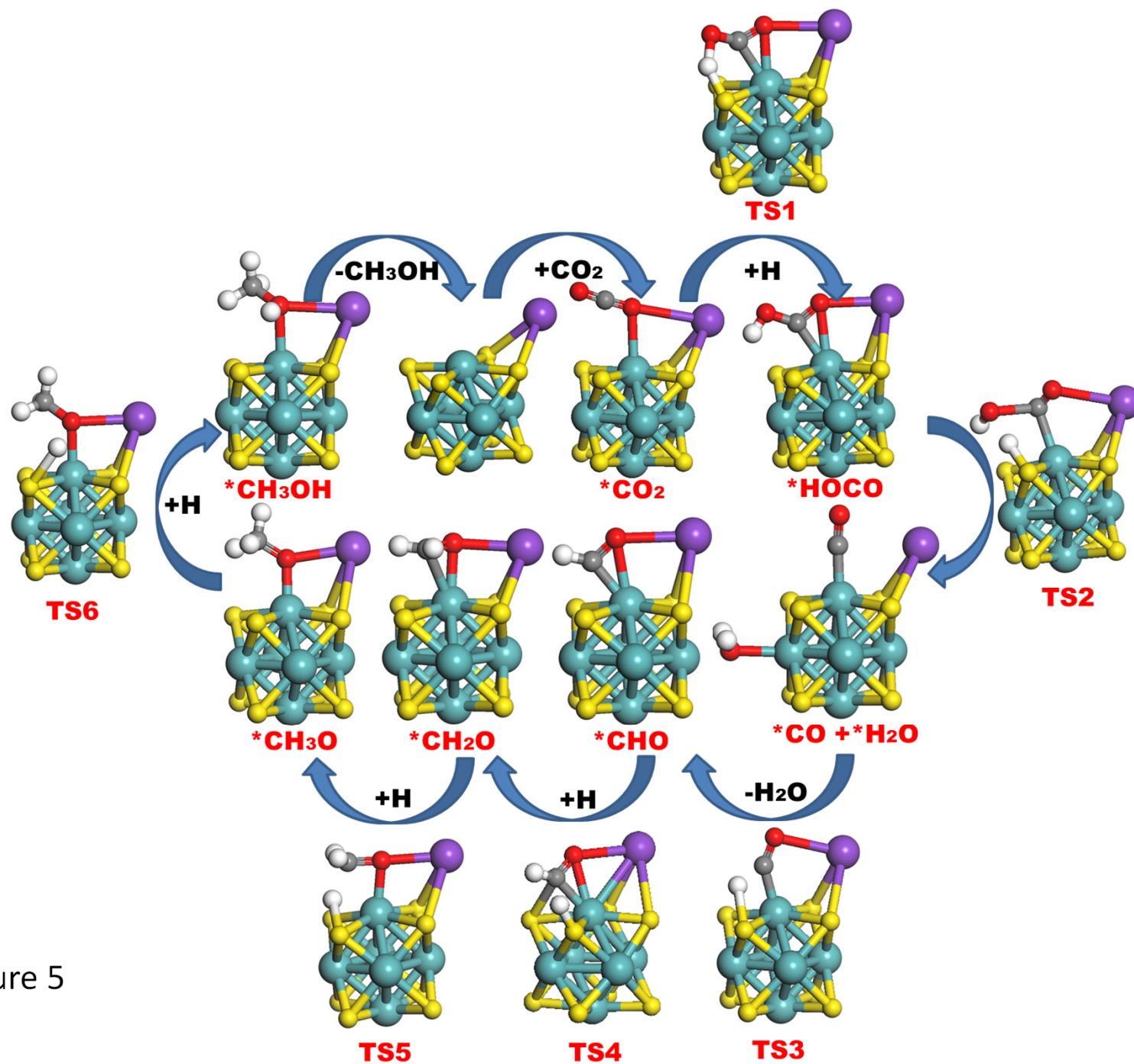


Figure 5

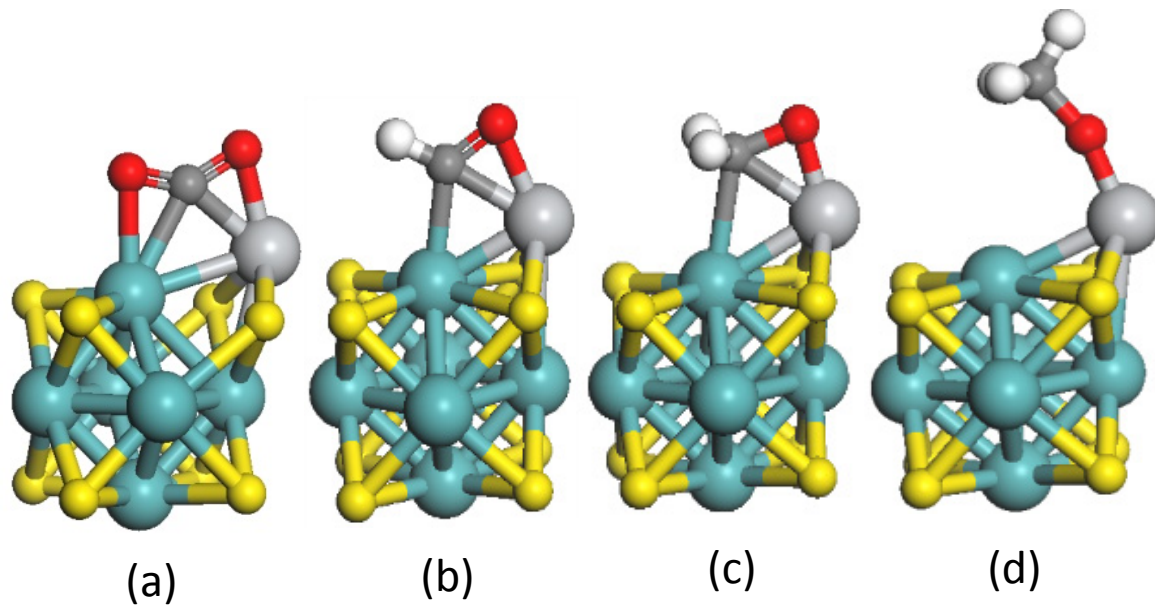


Figure 6

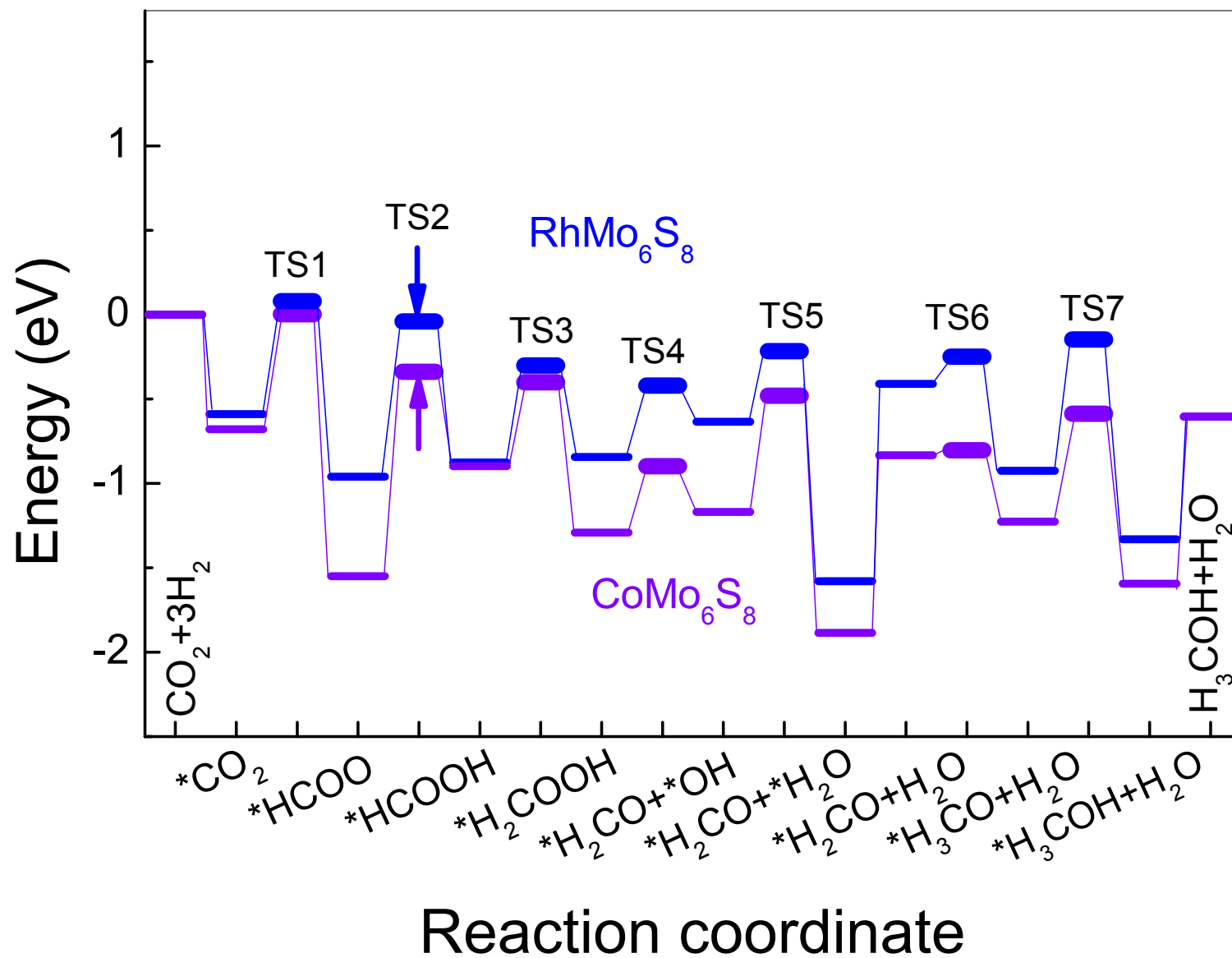


Figure 7

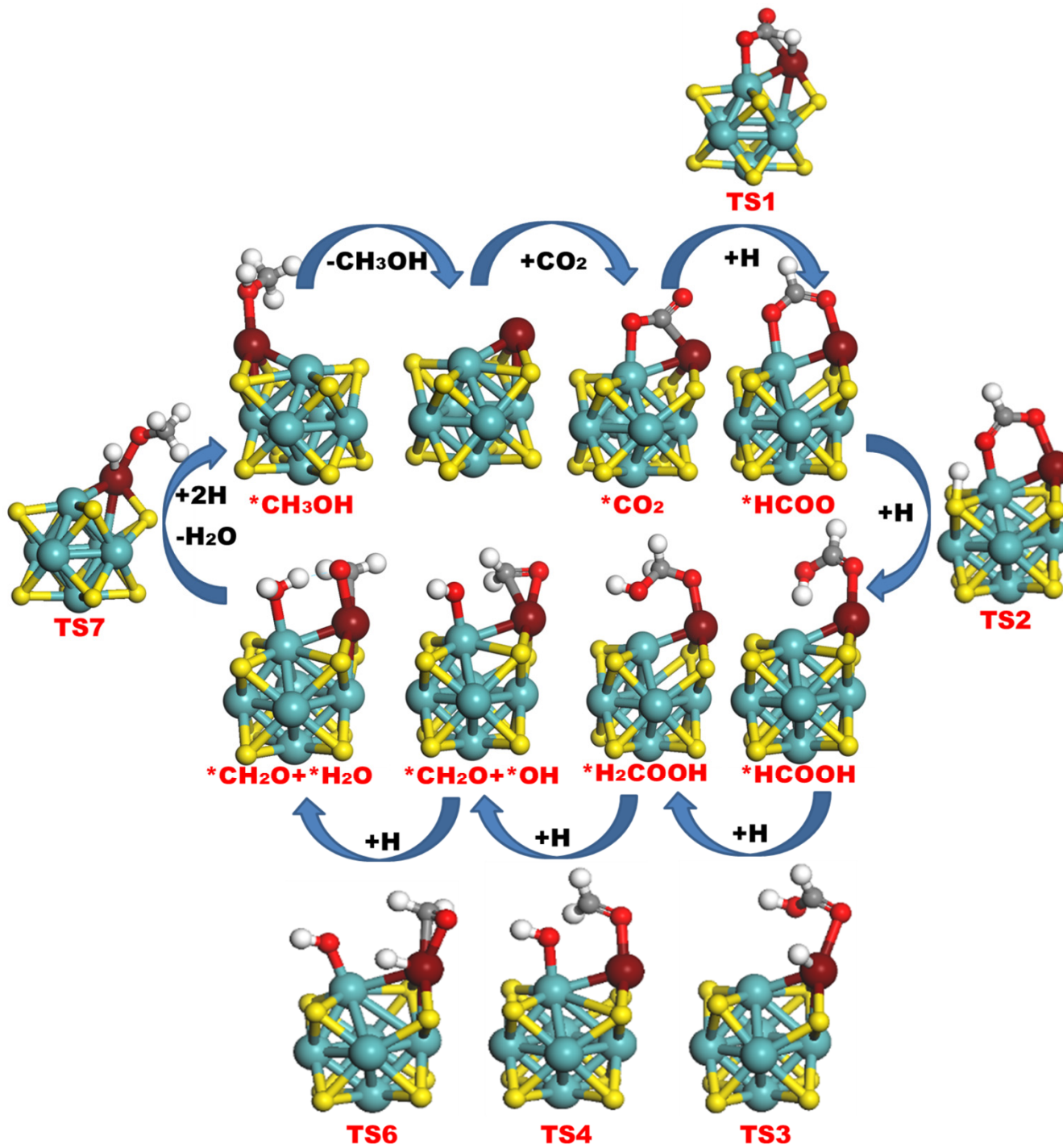


Figure 8

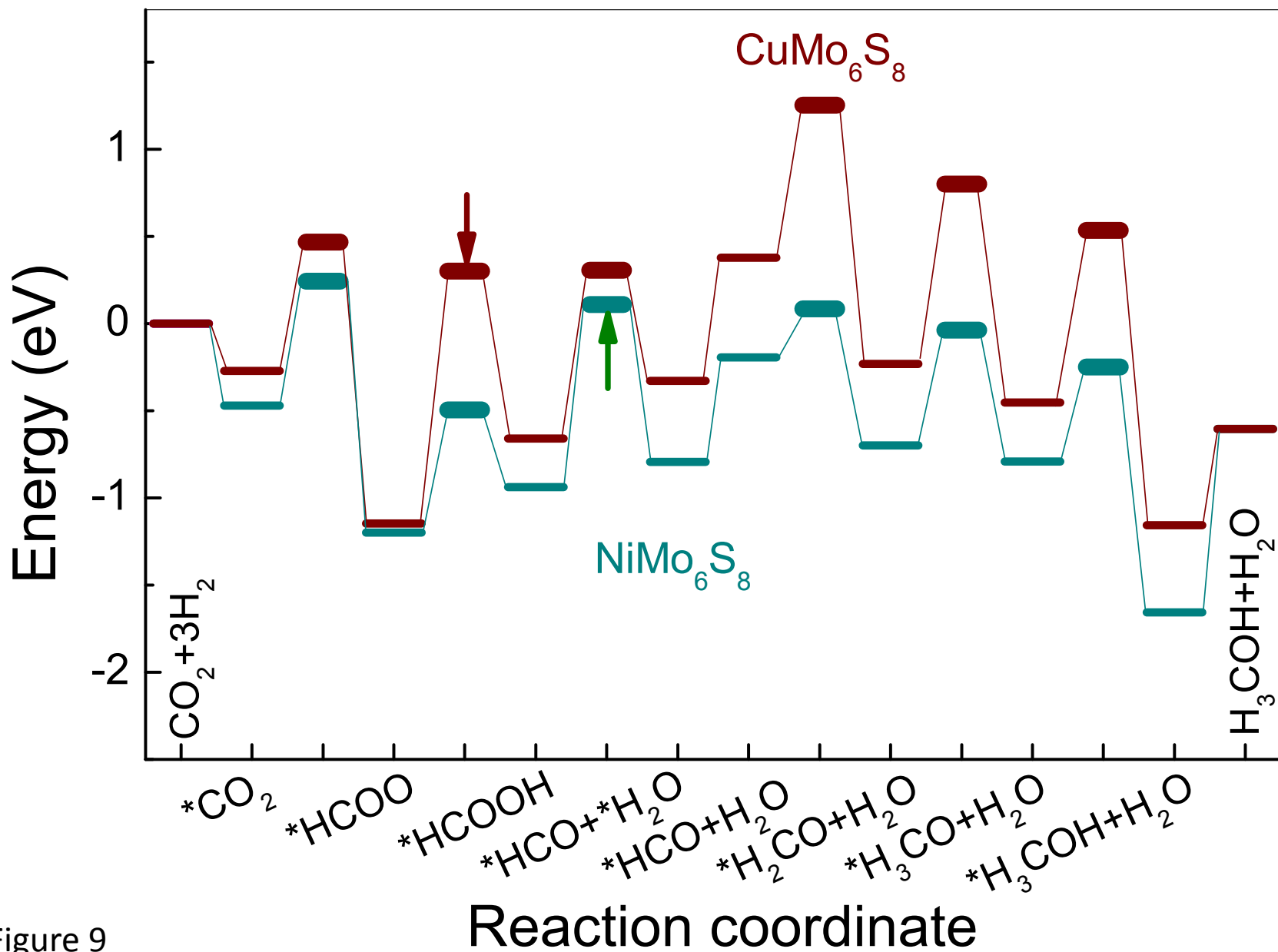
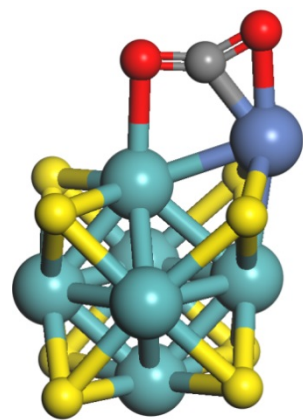
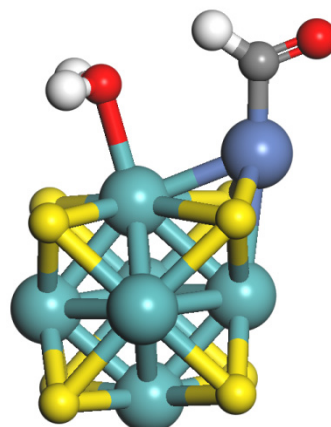


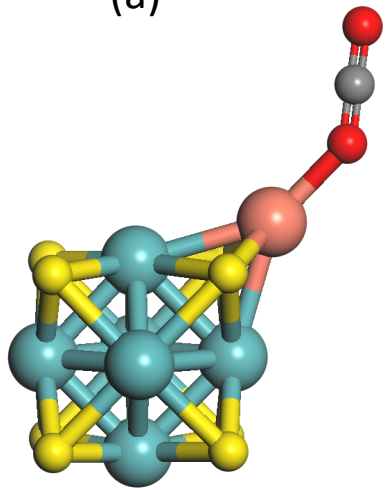
Figure 9



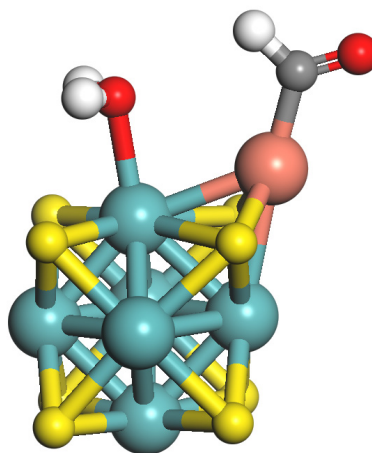
(a)



(b)



(c)



(d)

Figure 10

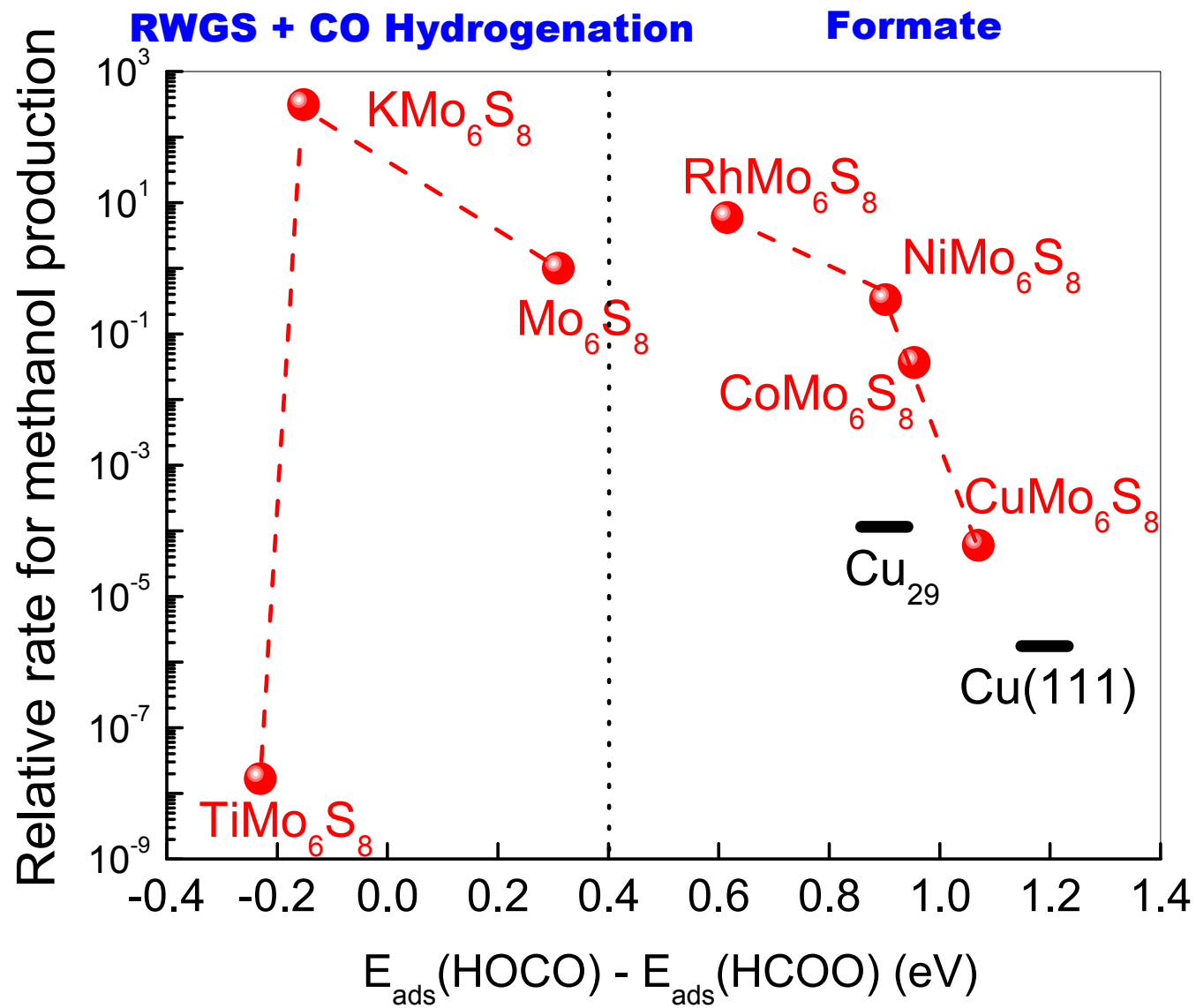
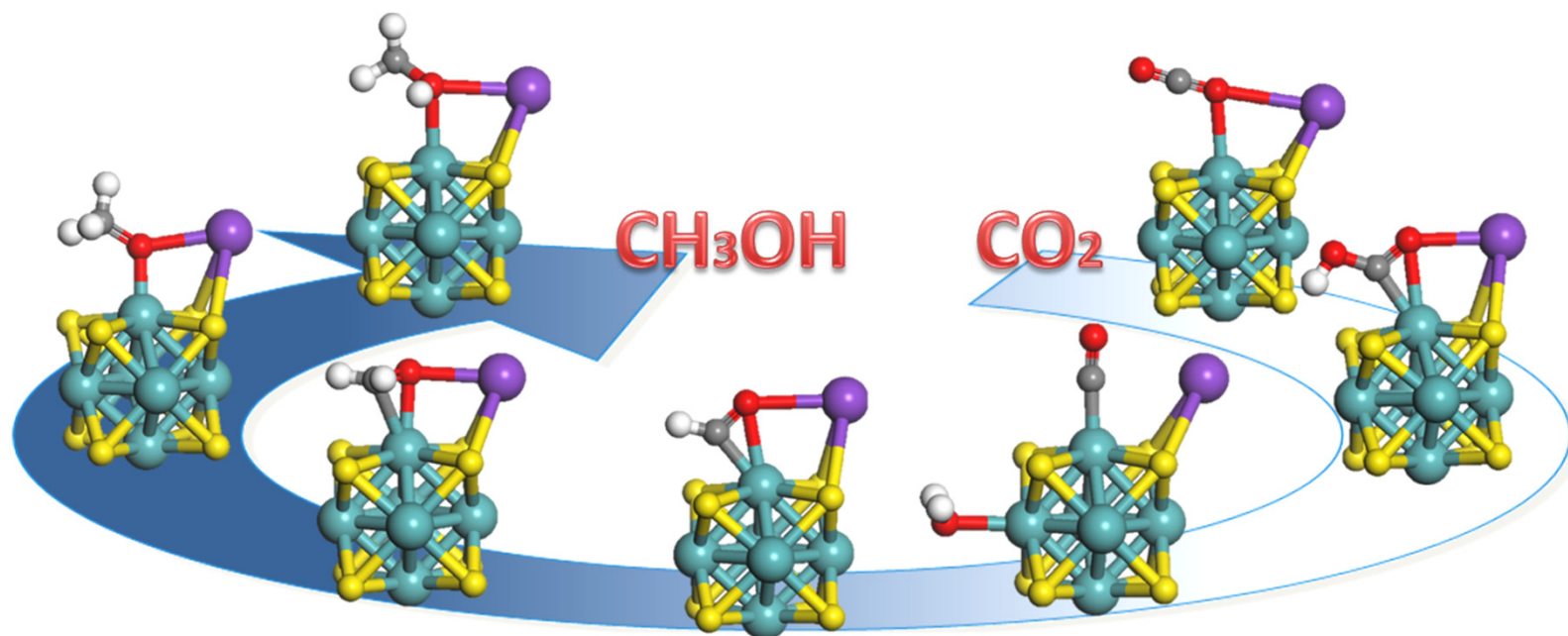


Figure 11

TOC



- (18) Zaman, S. F.; Smith, K. J. *Catal. Commun.* **2009**, *10*, 468.
- (19) Lee, J. S.; Kim, S.; Lee, K. H.; Nam, I.; Chung, J. S.; Kim, Y. G.; Woo, H. C. *Appl. Catal., A* **1994**, *110*, 11.
- (20) Huang, M.; Cho, K. *J. Phys. Chem. C* **2009**, *113*, 5238.
- (21) Subramani, V.; Gangwal, S. K. *Energy & Fuels* **2008**, *22*, 814.
- (22) Liu, P.; Choi, Y.; Yang, Y. X.; White, M. G. *J. Phys. Chem. A* **2010**, *114*, 3888.
- (23) Delley, B. *J. Chem. Phys.* **1990**, *92*, 508.
- (24) Delley, B. *J. Chem. Phys.* **2000**, *113*, 7756.
- (25) Perdew, J. P.; Burke, K.; Ernzerhof, M. *Phys. Rev. Lett.* **1996**, *77*, 3865.
- (26) Halgren, T. A.; Lipscomb, W. N. *Chem. Phys. Lett.* **1977**, *49*, 225.
- (27) Paskach, T. J.; Schrader, G. L.; McCarley, R. E. *J. Catal.* **2002**, *211*, 285.
- (28) Paskach, T. J.; Hilsenbeck, S. J.; Thompson, R. K.; McCarley, R. E.; Schrader, G. *L. J. Alloys Comp.* **2000**, *311*, 169.
- (29) Yvon, K. *Current Topics in Materials Science*; North-Holland Publishing,: Amsterdam, 1979; Vol. 3.
- (30) Seifert, G.; Tamuliene, J.; Gemming, S. *Comput. Mater. Sci.* **2006**, *35*, 316.
- (31) Murugan, P.; Kumar, V.; Kawazoe, Y.; Ota, N. *J. Phys. Chem. A* **2007**, *111*, 2778.
- (32) Patterson, M. J.; Lightstone, J. M.; White, M. G. *J. Phys. Chem. A* **2008**, *112*, 12011.
- (33) Kamiguchi, S.; Takeda, K.; Kajio, R.; Okumura, K.; Nagashima, S.; Chihara, T. *J. Clust. Sci.* **2013**, *24*, 559.
- (34) Shi, C.; Hansen, H. A.; Lausche, A. C.; Norskov, J. K. *Phys. Chem. Chem. Phys.* **2014**, *16*, 4720.
- (35) Kowal, A.; Li, M.; Shao, M.; Sasaki, K.; Vukmirovic, M. B.; Zhang, J.; Marinkovic, N. S.; Liu, P.; Frenkel, A. I.; Adzic, R. R. *Nature Mater.* **2009**, *8*, 325.
- (36) Choi, Y.; Liu, P. *J. Am. Chem. Soc.* **2009**, *131*, 13054.
- (37) Yang, L.; Liu, P. *Top. Catal.* **2014**, *57*, 125.
- (38) Askgaard, T. S.; Norskov, J. K.; Ovesen, C. V.; Stoltze, P. *J. Catal.* **1995**, *156*, 229.
- (39) Grabow, L. C.; Mavrikakis, M. *ACS Catal.* **2011**, *1*, 365.
- (40) Nørskov, J. K.; Rossmeisl, J.; Logadottir, A.; Lindqvist, L.; Kitchin, J.; Bligaard, T. *J. Phys. Chem. B* **2004**, *108*, 17886.
- (41) Sabatier, P. *Berichte der deutschen chemischen Gesellschaft* **1911**, *44*, 1984.
- (42) Lightstone, J. M.; Patterson, M. J.; White, M. G. *Chem. Phys. Lett.* **2005**, *413*, 429.